BIOCHEMISTRY
including biophysical chemistry & molecular biology

ARTICLE

pubs.acs.org/biochemistry

# A Conserved Surface Loop in Type I Dehydroquinate Dehydratases Positions an Active Site Arginine and Functions in Substrate Binding

Samuel H. Light,[†,‡] George Minasov,[†,‡] Ludmilla Shuvalova,[†,‡] Scott N. Peterson,[†,§] Michael Caffrey,[∥] Wayne F. Anderson,[†,‡] and Arnon Lavie*[,∥]

[†]Center for Structural Genomics of Infectious Diseases and [‡]Department of Molecular Pharmacology and Biological Chemistry, Feinberg School of Medicine, Northwestern University, Chicago, Illinois 60611, United States

[§]Pathogen Functional Genomics Resource Center, The J. Craig Venter Institute, 9712 Medical Center Drive, Rockville, Maryland 20850, United States

[∥]Department of Biochemistry and Molecular Genetics, University of Illinois, Chicago, Illinois 60607, United States

Supporting Information

**ABSTRACT:** Dehydroquinate dehydratase (DHQD) catalyzes the third step in the biosynthetic shikimate pathway. We present three crystal structures of the *Salmonella enterica* type I DHQD that address the functionality of a surface loop that is observed to close over the active site following substrate binding. Two wild-type structures with differing loop conformations and kinetic and structural studies of a mutant provide evidence of both direct and indirect mechanisms of involvement of the loop in substrate binding. In addition to allowing amino acid side chains to establish a direct interaction with the substrate, closure of the loop necessitates a conformational change of a key active site arginine, which in turn positions the substrate productively. The absence of DHQD in humans and its essentiality in many pathogenic bacteria make the enzyme a target for the development of nontoxic antimicrobials. The structures and ligand binding insights presented here may inform the design of novel type I DHQD inhibiting molecules.

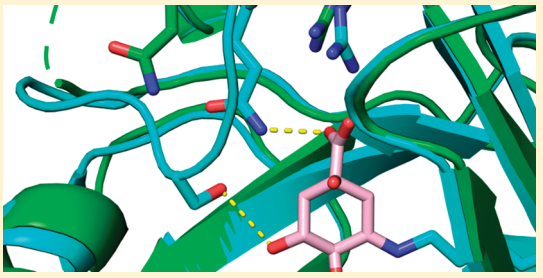

The seven enzymes of the shikimate pathway catalyze sequential reactions to generate chorismate, a crucial branch point in the synthesis of the aromatic amino acids.[1] Because of the essentiality of the shikimate pathway enzymes in a number of organisms and the absence of mammalian shikimate homologues, the shikimate pathway has been regarded as a viable target for the development of novel nontoxic antimicrobials, antifungals, and herbicides.[2−5]

The dehydration of dehydroquinate to dehydroshikimate represents the third step in the shikimate pathway (Figure 1). Biochemical and genetic studies have shown this reaction can be catalyzed by two phylogenetically unrelated enzyme families.[6] Type I dehydroquinate dehydratases (DHQDs) are found in plants, fungi, and some bacterial species.[7,8] In bacteria, these ∼29 kDa enzymes assemble into homodimers and catalyze a reaction that proceeds via a covalent Schiff base intermediate to result in a cis elimination.[9−11] Distinct from type I enzymes, type II DHQDs are found exclusively within bacteria. These ∼17 kDa enzymes assemble into homododecamers and catalyze a reaction that proceeds via a noncovalent enolate intermediate to result in a trans elimination.[12−14]

We recently reported crystal structures of the *Samonella enterica* type I DHQD in binary complex with the substrate 3-dehydroquinate in both a noncovalent pre-Schiff base state and a covalent Schiff base-bound reaction intermediate state.[15] In addition, we analyzed the *Clostridium difficile* type I DHQD in the covalent Schiff base-bound complex with the product 3-dehydroshikimate.[15] These crystal structures provided crucial insight into the reaction mechanism, suggesting that a single active site histidine cycles through multiple protonation events to catalyze the reaction and the formation and subsequent hydrolysis of the Schiff base intermediate.[15] Notably, these DHQD complexes consistently display a surface loop in a "closed" conformation that allows it to interact with the substrate or product. Here we report three substrate and ligand-free structures of *S. enterica* DHQD that reveal an "open" conformation of this surface loop. Along with a kinetic study of loop mutants, these new crystal structures establish two distinct functions for the surface loop, substrate binding and positioning an active site arginine residue, and demonstrate that appropriate loop function is vital to the DHQD-catalyzed reaction.

## EXPERIMENTAL PROCEDURES

**Cloning, Expression, and Purification of DHQD.** Standard Center for the Structural Genomics of Infectious Diseases protocols were used for cloning, overexpression, and purification

**Received:** December 20, 2010
**Revised:** February 1, 2011
**Published:** February 03, 2011

of *S. enterica* DHQD.[16] In short, *S. enterica* DHQD was cloned into the MCSG7 expression vector as previously described.[15] Following transformation into the BL21(DE3) *Escherichia coli* strain, cells were grown for 4 h at 37 °C. At that point, the temperature was reduced to 25 °C and protein overexpression induced by the addition of isopropyl 1-thio-D-galactopyranoside to a final concentration of 0.5 mM. After overnight growth, cells were harvested by centrifugation, resuspended in a buffer containing 10 mM Tris-HCl (pH 8.3), 500 mM NaCl, 10% glycerol, and 5 mM $\beta$-mercaptoethanol, and lysed by sonication. DHQD was purified by Ni-NTA affinity chromatography and eluted in a buffer containing 10 mM Tris-HCl (pH 8.3), 500 mM NaCl, and 5 mM $\beta$-mercaptoethanol. Immediately following purification, DHQD was concentrated to 7.5 mg/mL for crystallization screens.

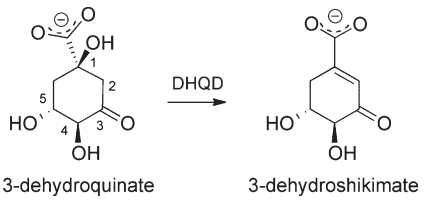


**Figure 1.** Reaction catalyzed by DHQD.

**Site-Directed Mutagenesis.** Following the supplier's technical manual, the QuikChange XL site-directed mutagenesis kit (Agilent) was used to generate S232A and Q236A variants; successful incorporation of mutations was confirmed by DNA sequencing.

**DHQD Activity Assay.** As previously described,[15] the DHQD bioactivity assay measured the increase in absorbance at a $\lambda$ of 234 nm to follow the formation of the conjugated enone carboxylate within dehydroshikimate ($\varepsilon$ = 12 $mM^{-1}$ $cm^{-1}$).[17]

**Protein Crystallization and Data Collection.** Sitting drop crystallization was set up at room temperature using a 1:1 ratio of DHQD to reservoir. Further details of the conditions of crystal growth are outlined in Table 1. Harvested crystals were transferred to mother liquor before being frozen in liquid nitrogen. Diffraction data were recorded at 100 K at the Life Sciences Collaborative Access Team at the Advance Photon Source (Argonne, IL).

**Structure Determination and Refinement.** All structural work was performed by the Center for Structural Genomics of Infectious Diseases.[18] Data were processed using HKL-3000 for indexing, integration, and scaling.[19] Structures were determined

**Table 1. Crystallization Conditions, Data Collection, and Refinement Statistics**

| | open loop $P2_12_12_1$ | closed loop $P2_1$ | Q236A |
|---|---|---|---|
| PDB entry | 3L2I | 3OEX | 3O1N |
| displayed color in figures | green | yellow | magenta |
| active site ligand | none | chloride | chloride |
| protein buffer solution | 500 mM NaCl and 10 mM Tris-HCl (pH 8.3) | 500 mM NaCl and 10 mM Tris-HCl (pH 8.3) | 500 mM NaCl and 10 mM Tris-HCl (pH 8.3) |
| crystallization condition | 200 mM $MgCl_2$ and 20% PEG 3350 | 170 mM $NH_4OAc$ (pH 4.6), 25.5% PEG 4000, and 15% glycerol | 200 mM $MgCl_2$, 100 mM Tris (pH 8.5), and 20% PEG 3350 |
| space group | $P2_12_12_1$ | $P2_1$ | $P1$ |
| unit cell dimensions | $a$ = 36.92 Å | $a$ = 69.26 Å | $a$ = 45.43 Å |
| | $b$ = 76.91 Å | $b$ = 75.76 Å | $b$ = 46.48 Å |
| | $c$ = 171.85 Å | $c$ = 99.90 Å | $c$ = 55.79 Å |
| | $\alpha$ = 90.00° | $\alpha$ = 90.00° | $\alpha$ = 104.23° |
| | $\beta$ = 90.00° | $\beta$ = 102.65° | $\beta$ = 97.50° |
| | $\gamma$ = 90.00° | $\gamma$ = 90.00° | $\gamma$ = 98.70° |
| resolution (Å) | 28.64−1.85 (1.90−1.85)[a] | 30.00−1.90 (1.93−1.90)[a] | 26.62−1.03 (1.05−1.03)[a] |
| no. of reflections | 42787 (3010)[a] | 69261 (3428)[a] | 196964 (8952)[a] |
| completeness (%) | 99.9 (98.6)[a] | 99.9 (99.7)[a] | 92.7 (84.9)[a] |
| redundancy | 6.5 (4.5)[a] | 3.3 (2.7)[a] | 4.3 (3.4)[a] |
| $R_{merge}I$ | 0.077 (0.355)[a] | 0.085 (0.398)[a] | 0.068 (0.333)[a] |
| $I/\sigma(I)$ | 21.3 (4.1)[a] | 12.6 (2.8)[a] | 15.0 (3.7)[a] |
| no. of molecules per asymmetric unit | 2 | 4 | 2 |
| no. of atoms | 4572 | 8540 | 4951 |
| $R_{work}/R_{free}$ | 0.168/0.214 | 0.152/0.204 | 0.140/0.161 |
| root-mean-square deviation | | | |
| bond lengths (Å) | 0.016 | 0.014 | 0.012 |
| bond angles (deg) | 1.526 | 1.431 | 1.464 |
| average $B$ factor | | | |
| protein | 23.1 | 23.2 | 14.2 |
| waters | 33.3 | 33.1 | 26.8 |
| ligand | − | 23.5 | 11.6 |

[a] Data for the highest-resolution shell in parentheses.

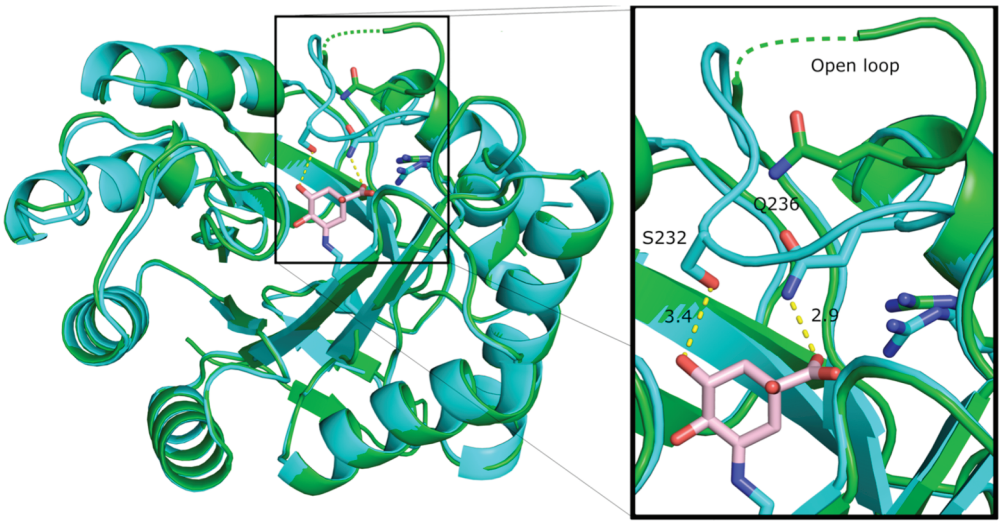


**Figure 2.** Dynamic loop behavior in DHQD. Overlay of open loop $P2_12_12_1$ (green) and predehydration intermediate-bound (cyan, PDB entry 3M7W) DHQD structures (rmsd of 0.28 Å over 198 Cα atoms, calculated with Val228−Gln236 residues omitted). A dashed green line traces where the disordered loop residues may lie. The inset highlights differential loop behavior between the two structures and shows interaction of the closed loop residues with the reaction intermediate (pink).

by molecular replacement using Phaser.[20] The *Salmonella typhi* apo DHQD structure (PDB entry 1GQN) was used as the starting model for the open loop $P2_12_12_1$ DHQD structure and the open loop $P2_12_12_1$ structure as a starting model for subsequently determined closed loop $P2_1$ and Q236A variant structures. Structures were refined with Refmac.[21] Models were displayed in Coot[22] and manually corrected on the basis of electron density maps. All structure figures were prepared using PyMOL Molecular Graphics System, version 1.3 (Schrödinger, LLC).

## RESULTS AND DISCUSSION

**Identification of a Surface Loop That Closes over the Active Site.** We recently reported crystal structures of the type I DHQD in which the substrate 3-dehydroquinate or the product 3-dehydroshikimate is covalently linked to Lys170 in pre- and postdehydration Schiff base-bound intermediate states.[15] To characterize additional functional states of the enzyme, we determined an apo state structure of the *S. enterica* DHQD in space group $P2_12_12_1$ (Table 1, open loop $P2_12_12_1$). A superposition of the apo structure with the previously reported reaction intermediate-bound crystal structure shows a mostly identical structural core (Figure 2). However, one significant difference is observed in residues spanning Val228−Gln236. In the apo structure, these residues are distant from the active site and residues Lys230−Ser232 could not be modeled because they display poor electron density (Figure S1a of the Supporting Information). In contrast, in the intermediate-bound structure, all residues in the region are well-ordered (Figure S1b of the Supporting Information) and are displaced to a position in which they form a side of the active site (Figure 2, inset).

Closure of this loop is likely due to the potential for formation of favorable hydrogen bonding interactions when substrate or product is bound. The reaction intermediate-bound structures reveal that in its closed conformation, side chains of loop residues Ser232 and Gln236 are within hydrogen bonding distance of the reaction intermediate's 5-hydroxyl and 1-carboxyl groups, respectively (Figure 2, inset). The ligand-responsive property of the surface loop observed in these crystal structures is consistent with previously reported type I DHQD structures from *Clostridium difficile*,[15] *S. typhi*,[10,23] *Staphylococcus aureus*,[24] *Aquifex aeolicus* (PDB entry 2YSW), *Geobacillus kaustophilus* (PDB entry 2YR1), and *Streptococcus pyogenes* (PDB entry 2OCZ), which display a similar open and/or disordered apo state and closed and ordered ligand-bound loop behavior. Similar behavior of this loop in multiple type I DHQDs suggests that inducible loop closure may be a general feature of substrate binding in these enzymes.

**Crystal Structure with Nonstandard Loop Behavior.** We determined a second DHQD structure in the absence of a biological ligand. Contrary to the open loop $P2_12_12_1$ crystal, this crystal adopted the $P2_1$ space group (Table 1, closed loop $P2_1$). Surprisingly, the behavior of the surface loop differs between these two crystal forms. Similar to the reaction intermediate-bound structures, all four molecules within the $P2_1$ asymmetric unit display a closed loop conformation (Figure S1c of the Supporting Information and Figure 3a). An overlay of these two structures reveals that in the $P2_1$ space group the open loop conformation would clash with residues from a crystallographic symmetry mate (Figure 3b). This suggests that adoption of the closed loop conformation may reflect constraints imposed by crystal packing rather than an accurate representation of solution state loop behavior in the absence of ligand.

Interestingly, within the closed loop $P2_1$ structure, a chloride from the crystallization buffer is observed at the enzyme's active site (Figure 4). An overlay of the closed loop $P2_1$ structure with the previously reported predehydration reaction intermediate-bound structure reveals that the chloride is bound in precisely the same position as the reaction intermediate's 1-carboxyl group (Figure 4). This observation provides a structural rationale for the previous report of this anion acting as a competitive inhibitor of type I DHQDs,[17] which was also found to be true of the *S. enterica* DHQD (data not shown). The absence of ordered chloride in other DHQD crystal structures, including our open loop $P2_12_12_1$ structure, despite crystallization conditions containing similarly

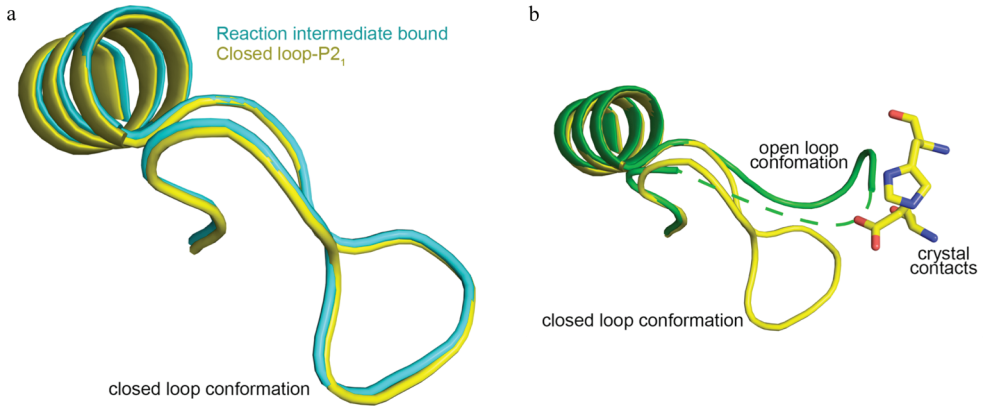


**Figure 3.** Closed loop conformation in the closed loop $P2_1$ structure likely resulting from crystal packing. (a) Superposition of predehydration intermediate-bound (cyan) and closed loop $P2_1$ (yellow) structures. The reaction intermediate is colored pink. (b) Superposition of the closed loop $P2_12_12_1$ (yellow) and open loop $P2_12_12_1$ (green) structures. Residues His51 and Glu89 of a symmetry-related molecule are proximal to the closed loop and would clash with an open loop conformation. A dashed green line traces where the disordered residues may lie.

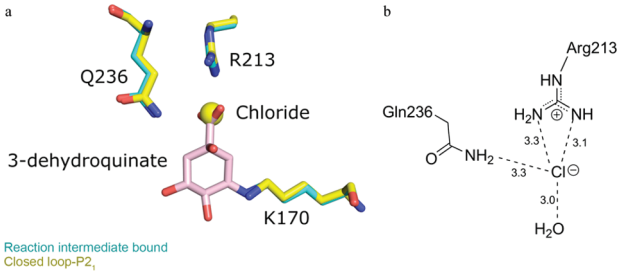


**Figure 4.** Chloride binding within the closed loop $P2_1$ active site. (a) Superposition of closed loop $P2_1$ (yellow) and predehydration reaction intermediate-bound (cyan) structures. The chloride and 1-carboxyl group localize to the same position within the active site. The reaction intermediate is colored pink. (b) Schematic representation of the closed loop $P2_1$ active site showing key chloride interactions.

high concentrations of the anion, suggests that chloride binding may be loop conformation-dependent; i.e., the anion may preferentially bind the closed loop state of the protein. This apparent requirement of loop closure for chloride binding, in combination with the similar localization of chloride and the 1-carboxyl group, suggests that a functional role of loop closure may be coordination of the substrate's anionic 1-carboxyl group to bind the substrate in a conformation conducive to catalysis.

**Catalytic Deficiencies of S232A and Q236A Loop Mutants.** Alignment of multiple DHQD surface loop sequences from distantly related organisms reveals a five-residue stretch of complete conservation (Figure 5a), implying a functionally significant role for this part of the loop. Notably, the two residues within this conserved stretch, Ser232 and Gln236, directly interact with the substrate or product (Figure 2, inset). To probe the function of these loop residues, we generated the Ser232 → Ala (S232A) and Gln236 → Ala (Q236A) mutants. The dehydration activity of wild-type (WT) and mutant enzymes was assayed, and Michaelis−Menten kinetics were determined (Table 2). Compared to the WT enzyme, both the S232A and Q236A variants have attenuated activity, which is reflected in both a decreased $k_{cat}$ and an increased $K_m$ (Table 2). While the S232A mutation results in a moderate 50-fold decrease in $k_{cat}/K_m$, the Q236A mutation results in a more severe 1000-fold decrease (Table 2).

The crystallographically observed interactions between Ser232 and Gln236 with the substrate or product indicate that both residues have a direct role in substrate binding. Because side chains of both Ser232 and Gln236 make a single interaction with the substrate, the residues might be expected to be similarly functionally important. However, the 20-fold lower efficiency of the Q236A mutant versus the S232A mutant implies a more critical role for Gln236 than Ser232 in the reaction and suggests that Gln236 may have a more extensive role than merely binding the substrate.

**Loop Closure Induces Conformational Change in Arg213.** Having identified a differential effect of the S232A and Q236A mutations on the enzyme's kinetics, we set out to identify the source of Ser232 and Gln236's differing functionalities. A comparison of apo and ligand-bound structures reveals that the transition from apo to reaction intermediate-bound states results in a conformational change in the Arg213 side chain (Figure 5b). This change is likely to be functionally significant because the residue moves from a position in the apo structure where its guanidinium group points away from the active site to a position in the reaction intermediate-bound structure where the guanidinium group forms a bidentate salt bridge with the reaction intermediate's 1-carboxyl group (Figure 5b).

Two features of Arg213's local environment differ between the apo and reaction intermediate-bound states, and thus, one or both are likely responsible for inducing the change in the conformation of Arg213. First, the presence of the reaction intermediate differs between the two structures. As such, substrate binding may bias Arg213 to a conformation in which the favorable interaction between its guanidinium and the substrate's 1-carboxyl group can form. Second, the loop conformation differs within the two structures. With the loop adopting its closed conformation, the apo conformation of Arg213 would be unusually close to loop residue Gln236 (Figure 5b). Thus, loop closure could produce an unfavorable Gln236−Arg213 clash if Arg213 did not change conformations. This latter possibility is particularly intriguing because, with the involvement of Gln236, it could explain the unexpectedly large effect of the Q236A mutation on the enzyme's kinetic parameters.

Because it isolates the effect of loop closure, the closed loop $P2_1$ structure allows for deconvolution of the relative influence of the two forces, substrate binding and loop closure, acting on Arg213.

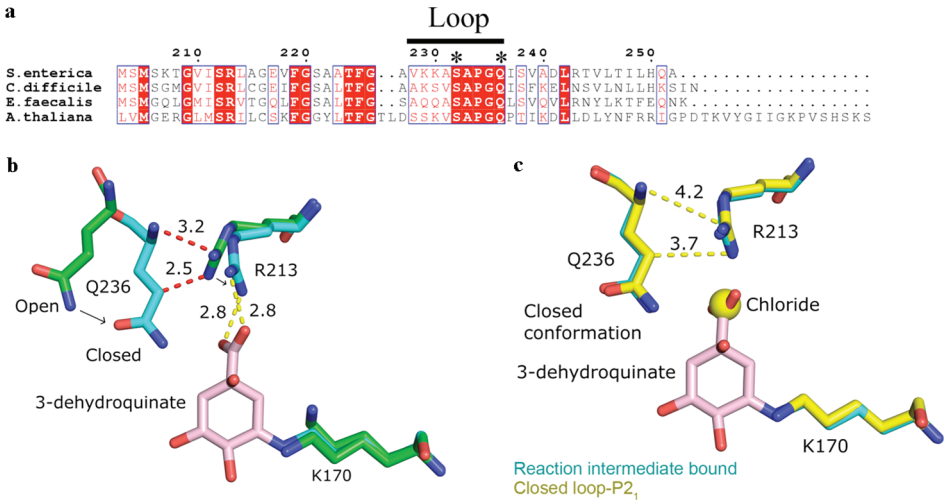


**Figure 5.** Loop closure results in a conformational change in Arg213. (a) Sequence alignment of the type I DHQDs from *S. enterica*, *C. difficile*, *Enterococcus faecalis*, and *Arabidopsis thaliana* done in ClustalW2 version 2 using ESPript version 2.2. Asterisks denote *S. enterica* Ser232 and Gln236, which are observed to hydrogen bond with the reaction intermediate. (b) Superposition of open loop $P2_12_12_1$ (green) and predehydration reaction intermediate-bound (cyan) active sites. The reaction intermediate-bound conformation of Arg213 positions the residue to form a bidentate salt bridge (yellow dashes) with the reaction intermediate's (pink) 1-carboxyl group. Distances that would be unusually short between the open loop $P2_12_12_1$ conformation of Arg213 and the reaction intermediate-bound conformation of Gln236 (red dashes) are given in angstroms. Arrows denote the direction of movement of Gln236 and Arg213 as the loop transitions from open to closed states. (c) Superposition of predehydration reaction intermediate (cyan) and closed loop $P2_1$ (yellow) structures. Arg213 adopts identical conformations in each structure.

**Table 2. Kinetic Characterization of WT, S232A, and Q236A DHQD**

| | $k_{cat}$ ($s^{-1}$) | $K_m$ ($\mu M$) | $k_{cat}/K_m$ ($s^{-1}\,\mu M^{-1}$) |
|---|---|---|---|
| WT | $210 \pm 5.1$ | $21 \pm 2.9$ | 10 |
| S232A | $107 \pm 7.4$ | $548 \pm 85$ | 0.20 |
| Q236A | $6.9 \pm 0.35$ | $682 \pm 204$ | 0.01 |

An analysis of this structure reveals that despite the absence of a biological ligand, when the loop is closed, Arg213 adopts its reaction intermediate-bound conformation (Figure 5c). Thus, even when the potential for formation of the guanidinium−carboxyl interaction is lacking, loop closure is sufficient to cause the Arg213 conformational change. This finding suggests that loop closure, and specifically the side chain of Gln236, may be critical for inducing the change in the conformation of Arg213.

**The Loop Mutant Fails To Induce a Conformational Change in Arg213.** A limitation in basing interpretations of the effect of loop closure on Arg213 conformation on the closed loop $P2_1$ structure results from the presence of chloride within this structure's active site. It is possible that the chloride has a compensatory effect for the absence of the 1-carboxyl group. In that case, it may be the presence of this anion rather than loop closure that is directly responsible for the change in Arg213 conformation. To address this possibility and to further probe the functional role of Gln236, we subjected the Q236A variant enzyme to crystallographic study.

Interestingly, the Q236A enzyme crystallized in a new crystal form that diffracted to a significantly higher resolution than any of the WT crystals (Table 1, Q236A variant). Analysis of this structure reveals that it behaves like a hybrid of the two WT structures. One molecule in this structure's asymmetric unit is similar to the WT open loop $P2_12_12_1$ structure and displays an open and partially disordered loop conformation (Figure S1d of the Supporting Information). The other molecule within the

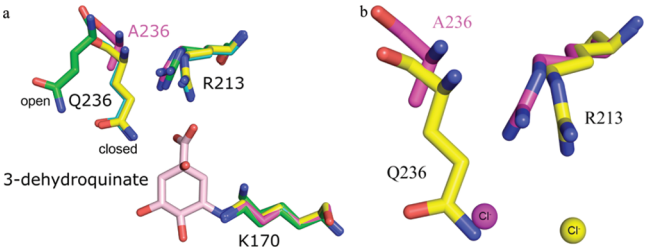


**Figure 6.** Q236A variant enzyme that fails to induce a conformational change in Arg213 and has altered anion coordinating properties. (a) Superposition of open loop $P2_12_12_1$ (green), predehydration reaction intermediate-bound (cyan), closed loop $P2_1$ (yellow), and closed loop Q236A (magenta) active sites. The reaction intermediate is colored pink. In both closed loop WT structures, Arg213 adopts its ligand-bound conformation. In the Q236A variant structure, Arg213 remains in its apo conformation. (b) Superposition of the closed loop $P2_1$ (yellow) and closed loop Q236A (magenta) active sites. Corresponding to the altered Arg213 conformation, the chloride is displaced 3.0 Å within the Q236A active site relative to its position in the WT enzyme.

asymmetric unit is similar to the WT closed loop $P2_1$ structure and, despite lacking the presence of biological ligand, adopts a closed loop conformation (Figure S1e of the Supporting Information). An examination of the mutant protein's crystal packing reveals that the open conformation of the closed loop is disallowed by precisely the same crystal packing as the WT closed loop $P2_1$ structure (Figure S2 of the Supporting Information). Also similar to behavior of the WT enzyme, the presence of chloride is observed within the asymmetric unit's closed loop but not its open loop molecule (Figure 6a). This correlation between loop conformation and active site chloride occupancy within a single crystal provides compelling evidence that chloride binding is loop conformation-dependent, providing further support for the idea that loop closure plays a key role in anion coordination. Despite cocrystallization and crystal soaking attempts,


dx.doi.org/10.1021/bi102020s |*Biochemistry* 2011, 50, 2357–2363

no biological ligand was observed in the Q236A variant active site, a result consistent with the mutant enzyme's increased $K_m$ (Table 2).

An overlay of the closed loop Q236A molecule with WT structures reveals that, despite loop closure, Arg213 remains in its apo conformation in the Q236A variant enzyme (Figure 6b). This finding allows the impact of Gln236 on Arg213 conformation to be deconvoluted from that of chloride. Because the Q236A variant enzyme is capable of binding chloride in its apo conformation, the possibility that the Arg213 conformational change observed in the WT closed loop $P2_1$ structure is a consequence of the chloride binding can be ruled out. Having eliminated this confounding variable, we can conclude that the differing Arg213 conformation between WT open loop $P2_12_12_1$ and closed loop $P2_1$ structures is the direct result of loop closure.

Furthermore, the difference in the conformation of Arg213 between WT closed loop $P2_1$ and closed loop Q236A structures demonstrates that Gln236 is the critical determinant responsible for loop closure's induction of the Arg213 conformational change. Without the side chain of Gln236, loop closure no longer results in a conformational change in Arg213. Thus, analysis of this structure establishes that (1) loop closure results in Arg213 adopting its substrate binding conformation and (2) Gln236 is the sole residue responsible for this conformational change.

The functional significance of the Q236A variant enzyme's inability to induce a conformational change in Arg213 is suggested by the behavior of the bound chloride anion. In the WT enzyme, the anion is coordinated by Arg213 and is positioned precisely where the substrate's 1-carboxyl group is found in the reaction intermediate-bound structures (Figure 4b). The similar localization of the 1-carboxyl group and chloride argues that Arg213 is likely to be functionally relevant for coordinating the 1-carboxyl group in the substrate binding event. In the closed loop Q236A structure, chloride is still coordinated by Arg213, but with the residue adopting its apo conformation, the anion is displaced ~3 Å (Figure 6c). Thus, without Gln236 inducing a change in the conformation of Arg213, the position of anion coordination shifts from the position of 1-carboxyl group binding to a position removed from the enzyme's catalytic center. Notably, if the 1-carboxyl group were to bind in the observed chloride position, then the substrate's 3-carbonyl carbon would be too far removed from the Schiff base forming Lys170 for formation of the covalent reaction intermediate to occur. As such, an inappropriate coordination of the carboxyl group to this position should greatly hinder enzyme activity.

In light of the evidence presented here, we propose that loop closure has two functions. First, as evidenced by the ligand-bound crystal structures and kinetic study of the S232A variant enzyme, loop residues directly interact with the substrate in a manner that facilitates substrate binding. Second, as demonstrated by structural and kinetic studies of the Q236A variant enzyme, loop closure and specifically Gln236 facilitate a conformational change in Arg213 that positions the residue to form a key interaction with the substrate's 1-carboxyl group. Thus, loop closure acts by both a direct and an indirect mechanism to facilitate substrate binding.

## CONCLUSIONS

We present three crystal structures of the type I *S. enterica* DHQD that address the function of a surface loop that is observed to close over the active site. An exception to the typical open and disordered apo state loop behavior, the first structure in which the loop adopts a closed conformation in the absence of substrate and/or product is presented. This structure demonstrates that loop closure results in a conformational change in the substrate binding residue Arg213. Kinetic studies of two mutants reveal that the loop is functionally important for catalysis. A crystal structure of the Q236A mutant enzyme demonstrates that Gln236 is required for loop closure to induce the conformational change in Arg213. A consequence of Arg213 forgoing its conformational change in this mutant is an ~3 Å shift in the position of chloride localization. The fact that the bound anion moves from the position of substrate carboxyl group binding to a position removed from the enzyme's catalytic center argues that Arg213's conformational change is critical for binding the 1-carboxyl group to position the substrate in the catalytically favored orientation. On the basis of the data presented here, we propose that the loop residues influence substrate binding by two separate mechanisms. Closure of the loop facilitates substrate binding by directly interacting with the substrate and by inducing a conformational change in Arg213 to its substrate binding position.

As a requisite step in aromatic amino acid biosynthesis, DHQD is a target for antimicrobial enzyme inhibitors. The findings presented here provide insight that may aid in targeted design of novel DHQD inhibitors. The attenuation of enzymatic activity resulting from compromised loop function validates an inhibition strategy based upon the prevention of loop closure, suggesting that a molecule capable of stabilizing the open state of the loop or destabilizing the closed state may be an effective allosteric DHQD inhibitor.

## ASSOCIATED CONTENT

**Supporting Information.** Model and associated electron density for the DHQD loop region from the structures discussed (Figure S1) and superposition of the open loop $P2_12_12_1$ and closed loop Q236A structures (Figure S2). This material is available free of charge via the Internet at http://pubs.acs.org.

### Accession Codes

Protein Data Bank entries 3L2I (open loop $P2_12_12_1$), 3OEX (closed loop $P2_1$), and 3O1N (Q236A variant).

## AUTHOR INFORMATION

### Corresponding Author

*Department of Biochemistry and Molecular Genetics, University of Illinois, 900 S. Ashland Ave., MBRB Room 1108, Chicago, IL 60607. Fax: (312) 355-4535. Telephone: (312) 355-5029. E-mail: lavie@uic.edu.

### Funding Sources

The Center for Structural Genomics of Infectious Diseases has been funded in whole or in part with federal funds from the National Institute of Allergy and Infectious Diseases, National Institutes of Health, Department of Health and Human Services, under Contract HHSN272200700058C (to W.F.A.). Use of the Advanced Photon Source at Argonne National Laboratory was supported by the U.S. Department of Energy, Office of Science, Office of Basic Energy Sciences, under Contract DE-AC02-06CH11357. Use of the LS-CAT Sector 21 was supported in part by the Michigan Economic Development Corp. and the

Michigan Technology Tri-Corridor for the support of this research program (Grant 085P1000817).

## ■ ACKNOWLEDGMENT

We thank Dr. Elisabetta Sabini for facilitating communication between groups involved in this work.

## ■ ABBREVIATIONS

DHQD, dehydroquinate dehydratase; Q236A, glutamine 236 → alanine DHQD variant; S232A, serine 232 → alanine DHQD variant; PDB, Protein Data Bank; WT, wild type.

## ■ REFERENCES

(1) Bentley, R. (1990) The shikimate pathway: A metabolic tree with many branches. *Crit. Rev. Biochem. Mol. Biol. 25*, 307–384.

(2) Benowitz, A. B., Hoover, J. L., and Payne, D. J. (2010) Antibacterial Drug Discovery in the Age of Resistance. *Microbe 5*, 390–396.

(3) Kishore, G. M., and Shah, D. M. (1988) Amino-Acid Biosynthesis Inhibitors as Herbicides. *Annu. Rev. Biochem. 57*, 627–663.

(4) Marques, M. R., Pereira, J. H., Oliveira, J. S., Basso, L. A., de Azevedo, W. F., Santos, D. S., and Palma, M. S. (2007) The inhibition of 5-enolpyruvylshikimate-3-phosphate synthase as a model for development of novel antimicrobials. *Curr. Drug Targets 8*, 445–457.

(5) Noble, M., Sinha, Y., Kolupaev, A., Demin, O., Earnshaw, D., Tobin, F., West, J., Martin, J. D., Qiu, C. Y., Liu, W. S., DeWolf, W. E., Tew, D., and Goryanin, I. I. (2006) The kinetic model of the shikimate pathway as a tool to optimize enzyme assays for high-throughput screening. *Biotechnol. Bioeng. 95*, 560–573.

(6) Kleanthous, C., Deka, R., Davis, K., Kelly, S. M., Cooper, A., Harding, S. E., Price, N. C., Hawkins, A. R., and Coggins, J. R. (1992) A comparison of the enzymological and biophysical properties of two distinct classes of dehydroquinase enzymes. *Biochem. J. 282* (Part 3), 687–695.

(7) Lumsden, J., and Coggins, J. R. (1977) Subunit Structure of Arom Multienzyme Complex of *Neurospora crassa*: Possible Pentafunctional Polypeptide Chain. *Biochem. J. 161*, 599–607.

(8) Polley, L. D. (1978) Purification and Characterization of 3-Dehydroquinate Hydrolase and Shikimate Oxidoreductase: Evidence for a Bifunctional Enzyme. *Biochim. Biophys. Acta 526*, 259–266.

(9) Butler, J. R., Alworth, W. L., and Nugent, M. J. (1974) Mechanism of Dehydroquinase Catalyzed Dehydration. 1. Formation of a Schiff-Base Intermediate. *J. Am. Chem. Soc. 96*, 1617–1618.

(10) Gourley, D. G., Shrive, A. K., Polikarpov, I., Krell, T., Coggins, J. R., Hawkins, A. R., Isaacs, N. W., and Sawyer, L. (1999) The two types of 3-dehydroquinase have distinct structures but catalyze the same overall reaction. *Nat. Struct. Biol. 6*, 521–525.

(11) Hanson, K. R., and Rose, I. A. (1963) Absolute Stereochemical Course of Citric Acid Biosynthesis. *Proc. Natl. Acad. Sci. U.S.A. 50*, 981–988.

(12) Price, N. C., Boam, D. J., Kelly, S. M., Duncan, D., Krell, T., Gourley, D. G., Coggins, J. R., Virden, R., and Hawkins, A. R. (1999) The folding and assembly of the dodecameric type II dehydroquinases. *Biochem. J. 338*, 195–202.

(13) Harris, J. M., Gonzalez-Bello, C., Kleanthous, C., Hawkins, A. R., Coggins, J. R., and Abell, C. (1996) Evidence from kinetic isotope studies for an enolate intermediate in the mechanism of type II dehydroquinases. *Biochem. J. 319* (Part 2), 333–336.

(14) Parker, E. J., Bello, C. G., Coggins, J. R., Hawkins, A. R., and Abell, C. (2000) Mechanistic studies on type I and type II dehydroquinase with (6R)- and (6S)-6-fluoro-3-dehydroquinic acids. *Bioorg. Med. Chem. Lett. 10*, 231–234.

(15) Light, S. H., Minasov, G., Shuvalova, L., Duban, M., Caffrey, M., Anderson, W. F., and Lavie, A. (2011) Insights into the mechanism of type I dehydroquinate dehydratases from structures of reaction intermediates. *J. Biol. Chem. 286*, 3531–3539.

(16) Kim, Y., Bigelow, L., Borovilos, M., Dementieva, I., Duggan, E., Eschenfeldt, W., Hatzos, C., Joachimiak, G., Li, H., Maltseva, N., Mulligan, R., Quartey, P., Sather, A., Stols, L., Volkart, L., Wu, R. Y., Zhou, M., and Joachimiak, A. (2008) High-Throughput Protein Purification for X-ray Crystallography and NMR. *Adv. Protein Chem. 75*, 85–105.

(17) Chaudhuri, S., Lambert, J. M., Mccoll, L. A., and Coggins, J. R. (1986) Purification and Characterization of 3-Dehydroquinase from *Escherichia coli*. *Biochem. J. 239*, 699–704.

(18) Anderson, W. F. (2009) Structural genomics and drug discovery for infectious diseases. *Infect. Disord.: Drug Targets 9*, 507–517.

(19) Otwinowski, Z., and Minor, W. (1997) Processing of X-ray diffraction data collected in oscillation mode. *Methods Enzymol. 276*, 307–326.

(20) McCoy, A. J., Grosse-Kunstleve, R. W., Storoni, L. C., and Read, R. J. (2005) Likelihood-enhanced fast translation functions. *Acta Crystallogr. D61*, 458–464.

(21) Murshudov, G. N., Vagin, A. A., Lebedev, A., Wilson, K. S., and Dodson, E. J. (1999) Efficient anisotropic refinement of macromolecular structures using FFT. *Acta Crystallogr. D55*, 247–255.

(22) Emsley, P., and Cowtan, K. (2004) Coot: Model-building tools for molecular graphics. *Acta Crystallogr. D60*, 2126–2132.

(23) Lee, W. H., Perles, L. A., Nagem, R. A., Shrive, A. K., Hawkins, A., Sawyer, L., and Polikarpov, I. (2002) Comparison of different crystal forms of 3-dehydroquinase from *Salmonella typhi* and its implication for the enzyme activity. *Acta Crystallogr. D58*, 798–804.

(24) Nichols, C. E., Lockyer, M., Hawkins, A. R., and Stammers, D. K. (2004) Crystal structures of *Staphylococcus aureus* type I dehydroquinase from enzyme turnover experiments. *Proteins 56*, 625–628.